

## Second-Order Nonlinear Optical Scattering Properties of Phosphine-Protected Au<sub>20</sub> Clusters

Stefan Knoppe,<sup>\*,†</sup> Qian-Fan Zhang,<sup>‡</sup> Xian-Kai Wan,<sup>§</sup> Quan-Ming Wang,<sup>§,||</sup> Lai-Sheng Wang,<sup>‡</sup> and Thierry Verbiest<sup>†</sup>

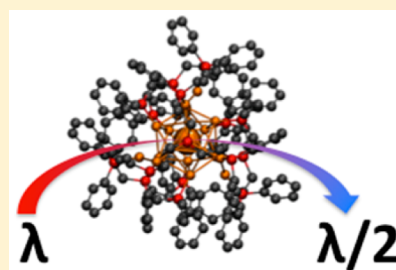
<sup>†</sup>Department of Chemistry, KU Leuven, Celestijnenlaan 200D, 3001 Leuven, Belgium

<sup>‡</sup>Department of Chemistry, Brown University, Providence, Rhode Island 02912, United States

<sup>§</sup>Department of Chemistry, Xiamen University, Xiamen, 361005, People's Republic of China

<sup>||</sup>Department of Chemistry, Tsinghua University, Beijing, 100084, People's Republic of China

**ABSTRACT:** We report the first hyperpolarizability of the [Au<sub>20</sub>(PP<sub>3</sub>)<sub>4</sub>]Cl<sub>4</sub> cluster (PP<sub>3</sub>: tris(2-(diphenylphosphino)ethyl)phosphine) using the Hyper-Rayleigh Scattering technique. This is the first determination of nonlinear optical properties of a phosphine-protected “superatomic” gold cluster. Weak contributions of multiphoton-excited fluorescence were observed in the spectral dispersion of the generated light upon excitation at 1300 and 1064 nm. The first hyperpolarizability of the intrinsically chiral cluster is weaker than that of thiolate-protected gold clusters of similar size and inherent chirality.



### ■ INTRODUCTION

Monolayer-protected metal clusters (MPCs) bridge the gap between small molecules and complexes containing only a few metal atoms and larger, metallic nanoparticles composed of thousands of metal atoms. MPCs typically contain several tens to a few hundred metal atoms.<sup>1</sup> Among MPCs, thiolate- and phosphine-protected gold clusters have been given the most attention, because of their exceptional stability in solution. Significant advances in synthesis,<sup>2,3</sup> isolation,<sup>4–6</sup> characterization,<sup>7,8</sup> and structure determination have been made in the past decade.<sup>9–16</sup> Their stability can be explained by delocalization of the valence electrons of the metal atoms (6s<sup>1</sup> in the case of gold) and formation of “superatomic complexes”.<sup>17</sup> MPCs bear potential for applications in catalysis<sup>18</sup> and sensing<sup>19,20</sup> and are ideally suited to study the emergence of the metallic state using bottom-up principles.

In 2003, Li et al. characterized a tetrahedral Au<sub>20</sub> cluster in the gas phase.<sup>21</sup> Subsequently, attempts have been made to prepare a ligand-protected analogue of this compound in solution.<sup>22</sup> Phosphine ligands were chosen, since thiolate ligands would alter the geometry and electronic structure of the parent T<sub>d</sub>-Au<sub>20</sub> cluster. Phosphine ligands are generally regarded more “innocent” in this respect. While mass spectrometry reveals the successful synthesis of clusters composed of 20 Au atoms and 4 (or 8) phosphine ligands, the structure of the cluster was not revealed by single-crystal X-ray crystallography. Substitution of two of the phenyl groups in triphenylphosphine by 2-pyridyl (bis(2-pyridyl)-phenylphosphine, PPhpy<sub>2</sub>) yields a 20-atom cluster as well. The structure of this cluster, [Au<sub>20</sub>(PPhpy<sub>2</sub>)<sub>10</sub>Cl<sub>4</sub>]Cl<sub>2</sub>, was solved by single-crystal structure determination and features a rodlike core.<sup>23</sup> The electronic structure of this cluster can be understood by

“superatomic bonding” of two 7-electron units (each of which being one electron short of the closest magic number, 8).<sup>24</sup> The formation of a rodlike structure (in contrast to the tetrahedral structure observed in the gas phase and assigned to the [Au<sub>20</sub>(PPh<sub>3</sub>)<sub>4</sub>]<sup>2+</sup> compound) is ascribed to interaction between the cluster core and the N atoms of the pyridyl groups. Thus, the ligand structure can have significant influence on the cluster structure.

Recently, the crystal structure of the [Au<sub>20</sub>(PP<sub>3</sub>)<sub>4</sub>]Cl<sub>4</sub> cluster (1) (PP<sub>3</sub>: tris(2-(diphenylphosphino)ethyl)phosphine) was determined independently by Wan et al.<sup>25</sup> and Chen et al.<sup>26</sup> In this case, the ligand is tetradentate. The cluster features a remarkable arrangement of the Au atoms, which form a centered icosahedron with a triblade Au<sub>7</sub> ad-motif (Figure 1). This ad-motif bestows chirality to the cluster. Since the ligand is achiral, the cluster is obtained as racemate, and the separation of its enantiomers has not been achieved to date. The electronic structure of 1 was explained as a 16-electron superatom complex,<sup>27</sup> with a superatomic orbital occupation of 1S<sup>2</sup> 1P<sup>6</sup> 1D<sup>6</sup> 2S<sup>2</sup>. The 1D orbitals are nondegenerate under the influence of the C<sub>3</sub> symmetry Au<sub>20</sub> core of the cluster, and the 2S level is stabilized.

Little is known about the nonlinear optical (NLO) properties of ligand-protected noble-metal clusters. Thiolate-protected gold clusters were identified as efficient two-photon absorbers.<sup>28,29</sup> Open-aperture z-scan measurements suggest a transition from molecule-like to plasmonic behavior in the

**Received:** August 1, 2016

**Revised:** September 14, 2016

**Accepted:** September 14, 2016

**Published:** September 14, 2016

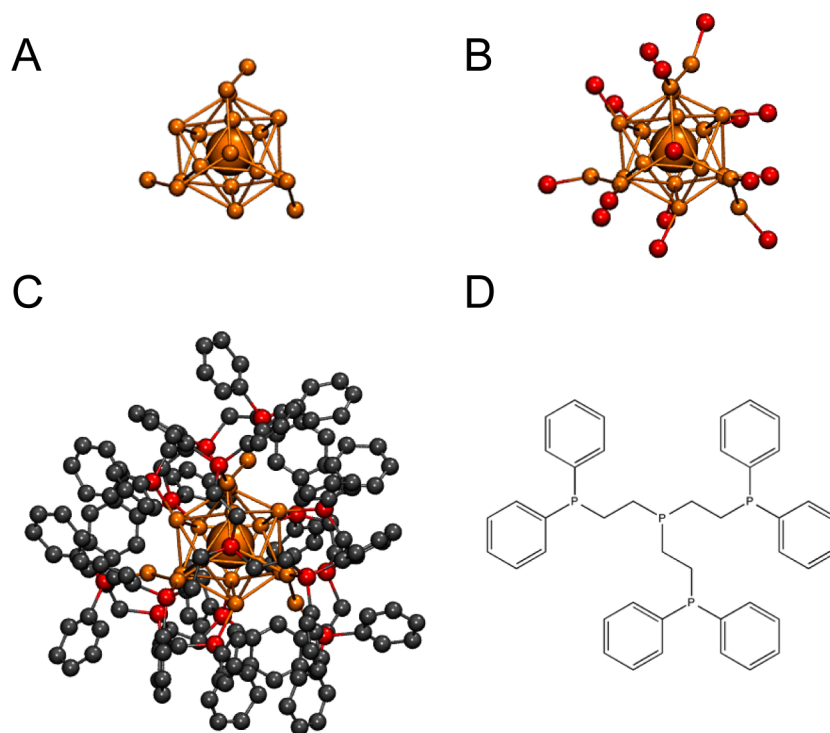


**Figure 1.** Structure of the  $[\text{Au}_{20}(\text{PP}_3)_4]^{4+}$  cluster. Coordinates are extracted from ref 25. (A) Arrangement of the Au atoms; the central atom is shown as a large sphere. The  $\text{Au}_7$  ad-motif is right-handed in this case. (B)  $\text{Au}_{20}\text{P}_{16}$  framework; phosphorus is shown in red. (C) The full  $[\text{Au}_{20}(\text{PP}_3)_4]^{4+}$  cluster; carbon is shown in gray, and hydrogen is not shown, for the sake of clarity. (D) Structure of the tris-(diphenylphosphino)ethylphosphine ( $\text{PP}_3$ ) ligand.

range of  $\text{Au}_{144}(\text{SR})_{60}$ ,<sup>30</sup> and transient absorption spectroscopy reveals metallic relaxation for this cluster.<sup>31,32</sup> Second-order nonlinear scattering was performed on small Au:thiolate clusters.<sup>33–35</sup> No correlation between the superatomic electron count of the cluster and the first hyperpolarizability  $\beta$  (a molecular measure for the efficiency of second-order nonlinear scattering) was found in a recent density functional theory (DFT) study; instead, the symmetry of the clusters dominates the first hyperpolarizability.<sup>36</sup> The NLO properties of thiolate-protected silver clusters recently have also become the focus of study.<sup>37–39</sup>

Here, we report on the second-order nonlinear light scattering properties of the  $[\text{Au}_{20}(\text{PP}_3)_4]\text{Cl}_4$  cluster. We determined the first hyperpolarizability  $\beta_{\text{HRS}}$  of the cluster using the Hyper-Rayleigh Scattering (HRS) method in solution.<sup>40</sup> To our knowledge, this is the first determination of NLO properties of phosphine-protected gold clusters.

## METHODS

**Synthesis of  $[\text{Au}_{20}(\text{PP}_3)_4]\text{Cl}_4$ .**  $[\text{Au}_{20}(\text{PP}_3)_4]\text{Cl}_4$  clusters were prepared according to a previously published protocol.<sup>26</sup> Analytical data (absorption spectra and mass spectrometry) are in agreement with previously published data.<sup>25,26</sup>

**Characterization.** Ultraviolet–visible–near-infrared (UV-vis-NIR) spectra were measured on a PerkinElmer Lambda 900 spectrophotometer. A cuvette of 10 mm path length was used. All spectra were measured in chloroform. For the determination of the molar extinction coefficient, a dilution series was measured.

**Hyper-Rayleigh Scattering.** All HRS measurements were carried out in chloroform. Before measurement, all solvents and samples were filtered over a syringe filter (polytetrafluoro-

ethylene (PTFE), 0.20  $\mu\text{m}$ ). Lambert–Beer correction terms were included (path length of 1 mm) in the analysis. All measurements were performed using a SpectraPhysics InsightDeepSee+ laser, at 1300 and 1064 nm. The collection optics are coupled to a Bruker 500is/sm spectrograph, together with an EMCCD camera (Andor Solis model iXon Ultra 897). As a calibration standard, neat  $\text{CHCl}_3$  was used. The first hyperpolarizability  $\beta_{\text{HRS}}$  of chloroform was taken from ref 41 ( $\beta_{\text{HRS},1064} = 0.208 \times 10^{-30}$  esu;  $\beta_{\text{HRS},1300} = 0.2000 \times 10^{-30}$ ). Errors of 10% were assumed for each measurement. The static hyperpolarizability was extrapolated using the following formula (two-state model):<sup>42</sup>

$$\beta_0 = \beta_{\text{laser}} \left[ 1 - \left( \frac{\lambda_{\text{max}}}{\lambda_{\text{laser}}} \right)^2 \right] \left[ 1 - \left( \frac{\lambda_{\text{max}}}{\lambda_{\text{HRS}}} \right)^2 \right]$$

where  $\lambda_{\text{laser}} = 1300$  and 1064 nm, respectively,  $\lambda_{\text{HRS}} = 650$  and 532 nm, respectively, and  $\lambda_{\text{max}} = 490$  nm.

**Density Functional Theory (DFT) Calculations.** DFT calculations were carried out using the ADF2014.01 software package.<sup>43</sup> Structures were optimized at the  $X\alpha/\text{TZP}$  level, and relativistic effects were included via the zeroth-order relativistic approximation (ZORA).<sup>44</sup> All optimizations were performed under vacuum. We used the coordinates provided in ref 25. We also consider model structures in which the phenyl groups of the ligands were replaced by H atoms and methyl groups. The optimized structures of cluster 1 are denoted as 1-H, 1-Me, and 1-Ph, respectively. The static first hyperpolarizability  $\beta_0$  was calculated using the LB94 model potential,<sup>45</sup> and the 27 tensor components  $\beta_{ijk}$  were averaged using the Kleinman formula<sup>46</sup> to yield the orientationally averaged  $\beta_{0,\text{HRS}}$ :

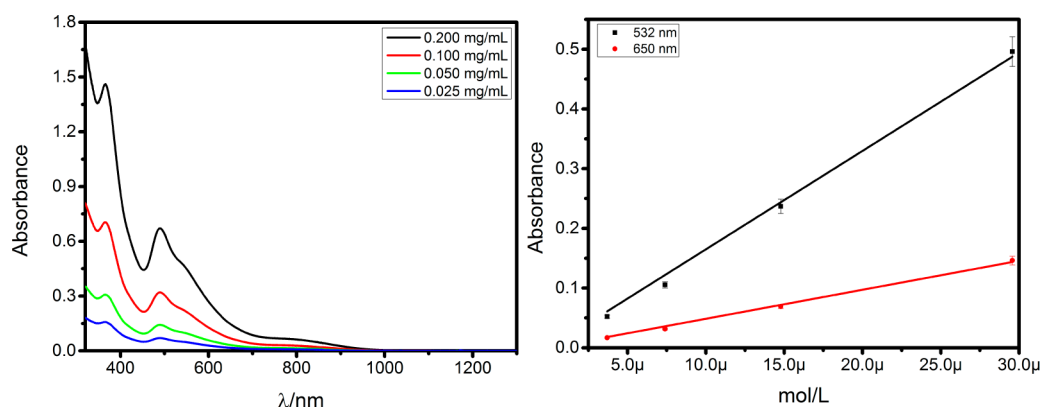


**Figure 2.** (Left) Absorption spectra of  $[\text{Au}_{20}(\text{PP}_3)_4]\text{Cl}_4$  in chloroform (10 mm) at different concentrations. (Right) Absorbance at 532 (black) and 650 nm (red) and their linear fit, as a function of concentration. The slopes reflect the molar extinction coefficients of  $16\,458$  and  $4858\text{ L mol}^{-1}\text{ cm}^{-1}$ , respectively.

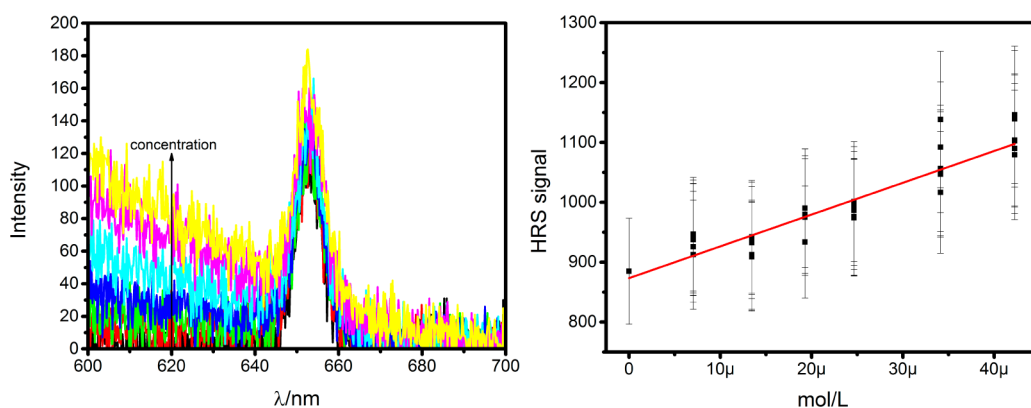


**Figure 3.** (Left) Hyper-Rayleigh Scattering (HRS) of  $[\text{Au}_{20}(\text{PP}_3)_4]\text{Cl}_4$  in chloroform upon excitation at  $1300\text{ nm}$ . The HRS peak centers at  $650\text{ nm}$  and increases in intensity with increasing concentration (the black trace is the pure solvent). The contribution from multiphoton-excited fluorescence is also observed. (Right) Linear fit of the HRS peak areas versus concentration of the cluster. The peak areas were corrected for reabsorption of the second-harmonic light at  $650\text{ nm}$ , using the Lambert–Beer law.

$$\langle \beta_{\text{HRS}}^2 \rangle = \langle \beta_{\text{ZZZ}}^2 \rangle + \langle \beta_{\text{XZZ}}^2 \rangle$$

where

$$\begin{aligned} \langle \beta_{\text{ZZZ}}^2 \rangle &= \frac{1}{7} \sum_i \beta_{\text{iii}}^2 + \frac{6}{35} \sum_{i \neq j} \beta_{\text{iii}} \beta_{\text{ijj}} + \frac{9}{35} \sum_{i \neq j} \beta_{\text{ijj}}^2 \\ &+ \frac{6}{35} \sum_{ijk, \text{cyclic}} \beta_{\text{ijj}} \beta_{\text{kkk}} + \frac{12}{35} \beta_{\text{ijk}}^2 \end{aligned}$$

and

$$\begin{aligned} \langle \beta_{\text{XZZ}}^2 \rangle &= \frac{1}{35} \sum_i \beta_{\text{iii}}^2 - \frac{2}{105} \sum_{i \neq j} \beta_{\text{iii}} \beta_{\text{ijj}} + \frac{11}{105} \sum_{i \neq j} \beta_{\text{ijj}}^2 \\ &- \frac{2}{105} \sum_{ijk, \text{cyclic}} \beta_{\text{ijj}} \beta_{\text{kkk}} + \frac{8}{35} \beta_{\text{ijk}}^2 \end{aligned}$$

The T = AB convention was used.<sup>47</sup>

## RESULTS AND DISCUSSION

The molar extinction coefficient of  $[\text{Au}_{20}(\text{PP}_3)_4]\text{Cl}_4$  was determined in chloroform by measurement of the absorption spectrum at four different concentrations (path length = 10 mm). Knowledge of the extinction coefficient at the second-harmonic wavelengths of 650 and 532 nm is important to correct the measured HRS signals for reabsorption (see below).

The absorption spectra show a distinct peak at 490 nm and shoulders at 535 and 755 nm, giving rise to ruby color in solution. The extinction coefficient at 532 nm is  $16\,458\text{ L cm}^{-1}\text{ mol}^{-1}$  and  $4858\text{ L cm}^{-1}\text{ mol}^{-1}$  at 650 nm (see Figure 2). These values are comparable to typical organic dyes. The onset of absorption is observed at 1000 nm. The influence of solvent could not be addressed since the cluster is exclusively soluble in chloroform and dichloromethane (for the latter, no significant influence is expected).

HRS was measured at two excitation wavelengths: 1300 and 1064 nm. This leads to second-order nonlinear scattering at 650 and 532 nm, respectively. Our instrument is capable of detecting the spectral dispersion of the light generated by NLO processes; thus, information about multiphoton-excited fluorescence is also available (the latter was not quantified).

When using an excitation wavelength of 1300 nm, a (weak) HRS signal is observed. The HRS signal is superimposed with that of the pure solvent and increases with concentration (Figure 3, left). The spectrum also reveals the contribution of a multiphoton-excited fluorescence signal. Since the maximum of the MPEF signal lies at a shorter wavelength than the second harmonic of the exciting laser, the emission is assumed to originate from a three-photon absorption process. Such a process has not been observed in MPCs of this size. The peak areas of the HRS signals were determined by fitting the measured spectra with Gaussian functions and integrating the HRS peaks centering at

650 nm. Next, the peak areas were corrected for reabsorption of the second-harmonic light assuming a path length of 1 mm. The corrected peak areas are linearly dependent on the concentration of the cluster (Figure 3, right). The first hyperpolarizability was then calculated from the slope of the peak areas versus the concentration using pure chloroform as an internal reference. A value of  $\beta_{\text{HRS},1300} = (55 \pm 5.5) \times 10^{-30}$  esu was calculated (Table 1).

**Table 1. First Hyperpolarizabilities of  $[\text{Au}_{20}(\text{PP}_{3,4})\text{Cl}_4]$  Determined at Fundamental Wavelengths of 1300 and 1064 nm<sup>a</sup>**

$\lambda$ (nm)	$\beta_{\lambda,\text{HRS}} (\times 10^{-30} \text{ esu})$	$\beta_{0,\text{HRS}} (\times 10^{-30} \text{ esu})$
1300	$55 \pm 5.5$	$20.5 \pm 2$
1064	$93 \pm 9.3$	$11.1 \pm 1$

<sup>a</sup>For extrapolation to the static hyperpolarizability, we used the extinction maximum at 490 nm.

When using an excitation wavelength of 1064 nm, linear correlation of the HRS signal with the concentration is observed when reabsorption of the second-harmonic light is considered (see Figure 4). This makes sense since the absorption of the cluster is  $\sim 3.4$  times stronger than at 1300 nm. Weak two-photon excited fluorescence centered at  $\sim 555$  nm is observed. A value of  $\beta_{\text{HRS},1064} = (93 \pm 9.3) \times 10^{-30}$  esu was calculated (Table 1). In order to confirm that the observed NLO effect is indeed a second-order process, we measured the dependence of the response on the laser intensity. For second-order processes, a quadratic dependence with the intensity is expected (or a linear dependence with the square of the normalized power,  $(P/P_{\text{max}})^2$ ). Such dependence is indeed observed (Figure 5). We did not succeed in measuring a similar dependence at 1300 nm, because of the low signal intensity observed, even at the highest laser power.

We also calculated the first hyperpolarizability of **1** using DFT. We consider three structures:

- (1) the phenyl groups in the cluster are replaced by hydrogen (**1-H**);
- (2) the phenyl groups were replaced by methyl groups (**1-Me**); and
- (3) the full cluster (**1-Ph**).

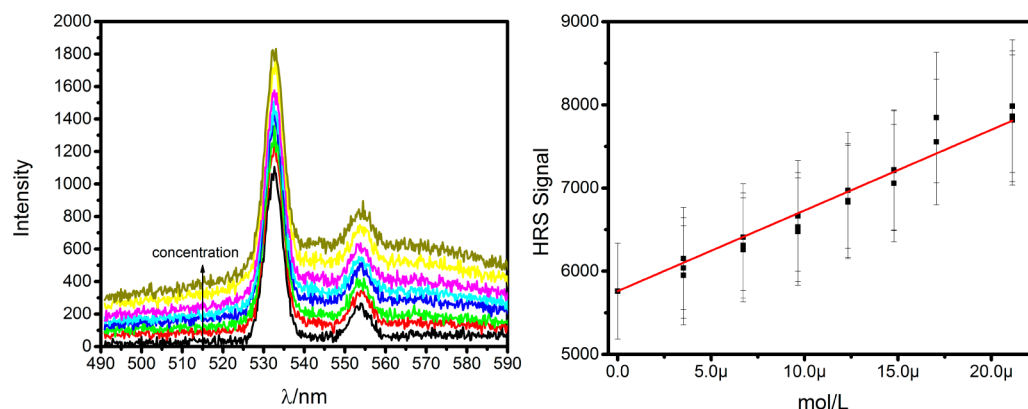


**Figure 4.** (Left) HRS of  $[\text{Au}_{20}(\text{PP}_{3,4})\text{Cl}_4]$  in chloroform upon excitation at 1064 nm. The HRS peak centers at 532 nm and increases in intensity with increasing concentration (the black trace is the pure solvent). The peak at 553 nm is the Hyper-Raman Scattering signal of the solvent. The contribution from multiphoton-excited fluorescence is also observed. (Right) Linear fit of the HRS peak areas versus concentration of the cluster. The peak areas were corrected for reabsorption of the second-harmonic light at 532 nm, using the Lambert–Beer law.

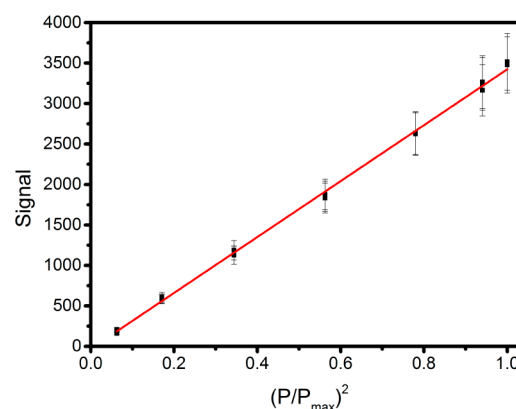


**Figure 5.** Dependence of the HRS signal with the square of the normalized laser power  $(P/P_{\text{max}})^2$  at 1064 nm. The linear correlation indicates that, indeed, a second-order nonlinear optical (NLO) process is observed (quadratic dependence on the laser intensity).

After geometry optimization, the static first hyperpolarizability  $\beta_{0,\text{HRS}}$ <sup>46</sup> was calculated using the LB94 functional and the DZP and TZP basis sets for **1-H** and **1-Me** and the DZP basis set for **1-Ph**. Details on the computational methods can be found in ref 36. The calculated first hyperpolarizabilities of **1-H** and **1-Me** are very similar (Table 2), indicating that the effect of these model ligands is negligible in this cluster. The differences between the DZP and TZP basis sets are negligible, which is due to the fact that ADF per default uses the TZP basis set for gold, instead of the requested DZP basis set. Thus, the smaller basis set is only used for carbon and phosphorus. Notably, the influence of methyl substitution, compared to hydrogen, is more subtle in the present case, while it is fairly drastic in thiolate-protected gold clusters.<sup>35</sup> The static first hyperpolarizability of **1-Ph** is significantly larger than those of **1-H** and **1-Me**, at least at the LB94/DZP level. We relate this to the fact that the aryl groups in the ligands can participate in the electronic structure of the gold cluster via  $\pi$ -acceptor interactions. Arylphosphines are better  $\pi$ -acceptors than alkylphosphines; this could expand the conjugated system and account for a larger hyperpolarizability.

We also included solvation effects on the first hyperpolarizability by using a COSMO solvent model<sup>48</sup> for chloroform ( $\epsilon_{\text{R}} = 4.8$ ). The inclusion of solvent effects leads

**Table 2.** Calculated Static First Hyperpolarizabilities of  $[\text{Au}_{20}(\text{PP}_3)_4]^{4+}$  (1)<sup>a</sup>

cluster	solvent	basis set	$\beta_{0,\text{HRS}} (\times 10^{-30} \text{ esu})$
1-H	vacuum	TZP	11.6
1-H	vacuum	DZP	10.61
1-H	$\text{CHCl}_3$	TZP	51.3
1-H	$\text{CHCl}_3$	DZP	46.6
1-Me	vacuum	TZP	11.1
1-Me	vacuum	DZP	10.85
1-Me	$\text{CHCl}_3$	TZP	38.5
1-Me	$\text{CHCl}_3$	DZP	37.2
1-Ph	vacuum	DZP	15.48
1-Ph	$\text{CHCl}_3$	DZP	66.1

<sup>a</sup>All values were calculated with the LB94 functional and DZP or TZP basis sets, using geometries obtained at the  $X\alpha/\text{TZP}$  level. Solvation effects (chloroform,  $\epsilon_{\text{R}} = 4.8$ ) were included using the COSMO model.

to improved accuracy of the calculated first hyperpolarizability of  $\text{Au}_{38}(\text{SCH}_3)_{24}$  clusters, when compared to the experiment.<sup>35</sup>

In order to compare the experimentally determined hyperpolarizabilities, we extrapolated the values at 1300 and 1064 nm to zero frequency, using the two-state model ( $\lambda_{\text{max}} = 490 \text{ nm}$ ).<sup>42</sup> The peak at 490 nm was ascribed to a core-ligand charge transfer band.<sup>27</sup> For excitation at 1300 nm, we obtain  $\beta_{0,\text{HRS}}$  values of  $(20.5 \pm 2) \times 10^{-30} \text{ esu}$  and  $(11.1 \pm 1) \times 10^{-30}$  for excitation at 1064 nm. This stark difference is due to the fact that, in both cases, the same absorption band was used as a reference. We acknowledge that the use of a two-state model may be inaccurate, since multiple transitions are observed in the absorption spectrum of the cluster. Regardless, both experimental values for  $\beta_{0,\text{HRS}}$  are well below the computed ones, especially when including solvation (Table 2). We suspect that the DFT method used here leads to severe overestimation of the first hyperpolarizability. Including solvation and methylthiolate model ligands leads to good agreement between computed and extrapolated (experimental) static hyperpolarizability in  $\text{Au}_{38}(\text{SR})_{24}$  clusters.<sup>35</sup> This indicates that phosphine ligands are less straightforward to treat computationally when it comes to the interaction with the cluster core. Furthermore, it is well-known that the choice of basis set is crucial when calculating nonlinear optical properties and diffuse functions should be included whenever possible.<sup>49</sup> However, the use of larger basis sets in huge systems, such as the title compound, is limited by the available computational resources. This prohibits usage of the QZ3P-nD basis set where diffuse functions would be included.

Comparison with thiolate-protected gold clusters is difficult, since only few experimental studies are available.<sup>33,35</sup>  $[\text{Au}_{25}(\text{SR})_{18}]^{-1}$  clusters protected with chiral thiolates (glutathione, captopril) yield values of the first hyperpolarizability between  $64 \times 10^{-30} \text{ esu}$  and  $163 \times 10^{-30} \text{ esu}$ , but we note that these were measured at excitation wavelengths of 1300 and 800 nm and, therefore, are not even directly comparable between themselves. In major contrast to the  $[\text{Au}_{20}(\text{PP}_3)_4]\text{Cl}_4$  cluster, the centrosymmetry of the  $[\text{Au}_{25}(\text{SR})_{18}]^{-1/0}$  clusters was broken using chiral ligands or doping with silver, whereas the title compound in the present study exhibits intrinsic chirality. The  $\text{Au}_{38}(\text{SCH}_2\text{CH}_2\text{Ph})_{24}$  cluster is intrinsically chiral and has a considerably larger hyperpolarizability ( $161 \times 10^{-30} \text{ esu}$ ).<sup>35</sup>

This indicates that phosphine ligands have significantly different influence on the second-order NLO properties than thiolates.

## CONCLUSION AND OUTLOOK

In summary, we determined the first hyperpolarizability of a phosphine-protected gold cluster for the first time using the Hyper-Rayleigh Scattering technique. The chosen cluster,  $[\text{Au}_{20}(\text{PP}_3)_4]\text{Cl}_4$ , is intrinsically chiral and therefore non-centrosymmetric. This leads to significant second-order nonlinear scattering. When using an excitation wavelength of 1300 nm, three-photon excited fluorescence is observed.

Since the available data for comparison are scarce, we suggest systematic studies on the influence of cluster size and composition (including the structure of the phosphine ligands) on the first hyperpolarizability to obtain a broader picture. This will also help in predicting trends regarding the transition from molecule-like clusters to larger nanoparticles, whose second-order nonlinear optical properties are of completely different origin.<sup>50</sup> Other ligand classes, such as selenolates<sup>51–53</sup> or alkynyl ligands,<sup>54–57</sup> also were recently used to protect noble-metal clusters, as well as mixtures of phosphines and thiolates.<sup>58,59</sup> The effects of these protection modes should be addressed in future studies as well.

## AUTHOR INFORMATION

### Corresponding Author

\*E-mail: stefan.knoppe@chem.kuleuven.be.

### Notes

The authors declare no competing financial interest.

## ACKNOWLEDGMENTS

We are grateful to KU Leuven and the Hercules Foundation for financial support. S.K. is a postdoctoral fellow of the “Funds for Academic Research—Flanders” (FWO). DFT calculations were carried out at “CSC—The IT Center for Science” (Espoo/Finland). We thank Hannu Häkkinen (University of Jyväskylä, Finland) for his support in carrying out the calculations. This contribution was identified by Hannu Häkkinen as the Best Presentation in the session “Nanometals” of the 2016 ACS Spring National Meeting in San Diego, CA.

## REFERENCES

- (1) Tsukuda, T.; Häkkinen, H. *Protected Metal Clusters: From Fundamentals to Applications*; Tsukuda, T., Häkkinen, H., Eds.; Elsevier: Amsterdam, 2015.
- (2) Brust, M.; Walker, M.; Bethell, D.; Schiffrin, D. J.; Whyman, R. Synthesis of Thiol-Derivatized Gold Nanoparticles in a Two-Phase Liquid-Liquid System. *J. Chem. Soc., Chem. Commun.* **1994**, 0, 801.
- (3) Jin, R.; Qian, H.; Wu, Z.; Zhu, Y.; Zhu, M.; Mohanty, A.; Garg, N. R. Size Focusing: A Methodology for Synthesizing Atomically Precise Gold Nanoclusters. *J. Phys. Chem. Lett.* **2010**, 1, 2903.
- (4) Negishi, Y.; Nobusada, K.; Tsukuda, T. Glutathione-Protected Gold Clusters Revisited: Bridging the Gap between Gold(I)-Thiolate Complexes and Thiolate-Protected Gold Nanocrystals. *J. Am. Chem. Soc.* **2005**, 127 (14), 5261.
- (5) Knoppe, S.; Boudon, J.; Dolamic, I.; Dass, A.; Bürgi, T. Size Exclusion Chromatography for Semipreparative Scale Separation of  $\text{Au}_{38}(\text{SR})_{24}$  and  $\text{Au}_{40}(\text{SR})_{24}$  and Larger Clusters. *Anal. Chem.* **2011**, 83, 5056–5061.
- (6) Dolamic, I.; Knoppe, S.; Dass, A.; Bürgi, T. First Enantioseparation and Circular Dichroism Spectra of  $\text{Au}_{38}$  Clusters Protected by Achiral Ligands. *Nat. Commun.* **2012**, 3, 798.
- (7) Dass, A.; Stevenson, A.; Dubay, G. R.; Tracy, J. B.; Murray, R. W. Nanoparticle MALDI-TOF Mass Spectrometry without Fragmenta-

- tion:  $\text{Au}_{25}(\text{SCH}_2\text{CH}_2\text{Ph})_{18}$  and Mixed Monolayer  $\text{Au}_{25}(\text{SCH}_2\text{CH}_2\text{Ph})_{18-x}(\text{L})_x$ . *J. Am. Chem. Soc.* **2008**, *130* (18), 5940.
- (8) Azubel, M.; Koivisto, J.; Malola, S.; Bushnell, D.; Hura, G. L.; Koh, A. L.; Tsunoyama, H.; Tsukuda, T.; Pettersson, M.; Häkkinen, H.; Kornberg, R. D. Electron Microscopy of Gold Nanoparticles at Atomic Resolution. *Science* **2014**, *345*, 909.
- (9) Jadzinsky, P. D.; Calero, G.; Ackerson, C. J.; Bushnell, D. A.; Kornberg, R. D. Structure of a Thiol Monolayer-Protected Gold Nanoparticle at 1.1 Å Resolution. *Science* **2007**, *318*, 430.
- (10) Heaven, M. W.; Dass, A.; White, P. S.; Holt, K. M.; Murray, R. W. Crystal Structure of the Gold Nanoparticle  $[\text{N}(\text{C}_8\text{H}_{17})_4]^-[\text{Au}_{25}(\text{SCH}_2\text{CH}_2\text{Ph})_{18}]^+$ . *J. Am. Chem. Soc.* **2008**, *130*, 3754.
- (11) Qian, H.; Eckenhoff, W. T.; Zhu, Y.; Pintauer, T.; Jin, R. Total Structure Determination of Thiolate-Protected  $\text{Au}_{38}$  Nanoparticles. *J. Am. Chem. Soc.* **2010**, *132*, 8280.
- (12) Crasto, D.; Malola, S.; Brososky, G.; Dass, A.; Häkkinen, H. Single Crystal XRD Structure and Theoretical Analysis of the Chiral  $\text{Au}_{30}\text{S}(\text{S-T-Bu})_{18}$  Cluster. *J. Am. Chem. Soc.* **2014**, *136*, 5000.
- (13) Zeng, C.; Qian, H.; Li, T.; Li, G.; Rosi, N. L.; Yoon, B.; Barnett, R. N.; Whetten, R. L.; Landman, U.; Jin, R. Total Structure and Electronic Properties of the Gold Nanocrystal  $\text{Au}_{36}(\text{SR})_{24}$ . *Angew. Chem., Int. Ed.* **2012**, *51*, 13114.
- (14) Zeng, C.; Li, T.; Das, A.; Rosi, N. L.; Jin, R. Chiral Structure of Thiolate-Protected 28-Gold-Atom Nanocluster Determined by X-ray Crystallography. *J. Am. Chem. Soc.* **2013**, *135*, 10011.
- (15) Zeng, C.; Chen, Y.; Kirschbaum, K.; Appavoo, K.; Sfeir, M. Y.; Jin, R. Structural Patterns at All Scales in a Nonmetallic Chiral  $\text{Au}_{133}(\text{SR})_{52}$  Nanoparticle. *Sci. Adv.* **2015**, *1*, e1500045.
- (16) Dass, A.; Theivendran, S.; Nimmala, P. R.; Kumara, C.; Jupally, V. R.; Fortunelli, A.; Sementa, L.; Barcaro, G.; Zuo, X.; Noll, B. C.  $\text{Au}_{133}(\text{SPh-t-Bu})_{52}$  Nanomolecules: X-Ray Crystallography, Optical, Electrochemical, and Theoretical Analysis. *J. Am. Chem. Soc.* **2015**, *137*, 4610.
- (17) Walter, M.; Akola, J.; Lopez-Acevedo, O.; Jadzinsky, P. D.; Calero, G.; Ackerson, C. J.; Whetten, R. L.; Grönbeck, H.; Häkkinen, H. A Unified View of Ligand-Protected Gold Clusters as Superatom Complexes. *Proc. Natl. Acad. Sci. U. S. A.* **2008**, *105*, 9157.
- (18) Li, G.; Jin, R. Atomically Precise Gold Nanoclusters as New Model Catalysts. *Acc. Chem. Res.* **2013**, *46*, 1749.
- (19) Marjomäki, V.; Lahtinen, T.; Martikainen, M.; Koivisto, J.; Malola, S.; Salorinne, K.; Pettersson, M.; Häkkinen, H. Site-Specific Targeting of Enterovirus Capsid by Functionalized Monodisperse Gold Nanoclusters. *Proc. Natl. Acad. Sci. U. S. A.* **2014**, *111*, 1277.
- (20) Chen, L.-Y.; Wang, C.-W.; Yuan, Z.; Chang, H.-T. Fluorescent Gold Nanoclusters: Recent Advances in Sensing and Imaging. *Anal. Chem.* **2015**, *87*, 216.
- (21) Li, J.; Li, X.; Zhai, H. J.; Wang, L. S.  $\text{Au}_{20}$ : A Tetrahedral Cluster. *Science* **2003**, *299*, 864.
- (22) Zhang, H. F.; Stender, M.; Zhang, R.; Wang, C.; Li, J.; Wang, L. S. Toward the Solution Synthesis of the Tetrahedral  $\text{Au}_{20}$  Cluster. *J. Phys. Chem. B* **2004**, *108*, 12259.
- (23) Wan, X. K.; Lin, Z. W.; Wang, Q. M.  $\text{Au}_{20}$  Nanocluster Protected by Hemilabile Phosphines. *J. Am. Chem. Soc.* **2012**, *134*, 14750.
- (24) Yuan, Y.; Cheng, L.; Yang, J. Electronic Stability of Phosphine-Protected  $\text{Au}_{20}$  Nanocluster: Superatomic Bonding. *J. Phys. Chem. C* **2013**, *117*, 13276.
- (25) Wan, X. K.; Yuan, S. F.; Lin, Z. W.; Wang, Q. M. A Chiral Gold Nanocluster  $\text{Au}_{20}$  Protected by Tetradentate Phosphine Ligands. *Angew. Chem., Int. Ed.* **2014**, *53*, 2923.
- (26) Chen, J.; Zhang, Q. F.; Williard, P. G.; Wang, L. S. Synthesis and Structure Determination of a New  $\text{Au}_{20}$  Nanocluster Protected by Tripodal Tetrakisphosphine Ligands. *Inorg. Chem.* **2014**, *53*, 3932.
- (27) Knoppe, S.; Lehtovaara, L.; Häkkinen, H. Electronic Structure and Optical Properties of the Intrinsically Chiral 16-Electron Superatom Complex  $[\text{Au}_{20}(\text{PP}_3)_4]^{4+}$ . *J. Phys. Chem. A* **2014**, *118*, 4214.
- (28) Ramakrishna, G.; Varnavski, O.; Kim, J.; Lee, D.; Goodson, T. Quantum-Sized Gold Clusters as Efficient Two-Photon Absorbers. *J. Am. Chem. Soc.* **2008**, *130*, 5032.
- (29) Day, P. N.; Nguyen, K. A.; Pachter, R. Calculation of One- and Two-Photon Absorption Spectra of Thiolated Gold Nanoclusters Using Time-Dependent Density Functional Theory. *J. Chem. Theory Comput.* **2010**, *6*, 2809.
- (30) Philip, R.; Chantharasupawong, P.; Qian, H.; Jin, R.; Thomas, J. Evolution of Nonlinear Optical Properties: From Gold Atomic Clusters to Plasmonic Nanocrystals. *Nano Lett.* **2012**, *12*, 4661.
- (31) Yi, C.; Tofanelli, M. A.; Ackerson, C. J.; Knappenberger, K. L. Optical Properties and Electronic Energy Relaxation of Metallic  $\text{Au}_{144}(\text{SR})_{60}$  Nanoclusters. *J. Am. Chem. Soc.* **2013**, *135*, 18222.
- (32) Yi, C.; Zheng, H.; Tvedte, L. M.; Ackerson, C. J.; Knappenberger, K. L. Nanometals: Identifying the Onset of Metallic Relaxation Dynamics in Monolayer-Protected Gold Clusters Using Femtosecond Spectroscopy. *J. Phys. Chem. C* **2015**, *119*, 6307.
- (33) Russier-Antoine, I.; Bertorelle, F.; Vojkovic, M.; Rayane, D.; Salmon, E.; Jonin, C.; Dugourd, P.; Antoine, R.; Brevet, P.-F. Non-Linear Optical Properties of Gold Quantum Clusters. The Smaller the Better. *Nanoscale* **2014**, *6*, 13572.
- (34) Knoppe, S.; Vanbel, M. K.; Van Cleuvenbergen, S. J.; Vanpraet, L.; Bürgi, T.; Verbiest, T. Nonlinear Optical Properties of Thiolate-Protected Gold Clusters. *J. Phys. Chem. C* **2015**, *119*, 6221.
- (35) van Steerteghem, N.; Van Cleuvenbergen, S. J.; Deckers, S.; Kumara, C.; Dass, A.; Häkkinen, H.; Clays, K.; Verbiest, T.; Knoppe, S. Symmetry Breaking in Ligand-Protected Metal Clusters Probed by Hyper-Rayleigh Scattering. *Nanoscale* **2016**, *8*, 12123.
- (36) Knoppe, S.; Häkkinen, H.; Verbiest, T. Nonlinear Optical Properties of Thiolate-Protected Gold Clusters: A Theoretical Survey of the First Hyperpolarizabilities. *J. Phys. Chem. C* **2015**, *119*, 27676.
- (37) Sanader, Ž.; Krstić, M.; Russier-Antoine, I.; Bertorelle, F.; Dugourd, P.; Brevet, P.-F.; Antoine, R.; Bonačić-Koutecký, V. Two-Photon Absorption of Ligand-Protected  $\text{Ag}_{15}$  Nanoclusters. Towards a New Class of Nonlinear Optics Nanomaterials. *Phys. Chem. Chem. Phys.* **2016**, *18*, 12404–12408.
- (38) Day, P. N.; Pachter, R.; Nguyen, K. A.; Bigioni, T. P. Linear and Nonlinear Optical Response in Silver Nanoclusters: Insight from a Computational Investigation. *J. Phys. Chem. A* **2016**, *120*, 507.
- (39) Russier-Antoine, I.; Bertorelle, F.; Hamouda, R.; Rayane, D.; Dugourd, P.; Sanader, Z.; Bonačić-Koutecký, V.; Brevet, P.-F.; Antoine, R. Tuning  $\text{Ag}_{29}$  Nanocluster Light Emission from Red to Blue with One and Two-Photon Excitation. *Nanoscale* **2016**, *8*, 2892.
- (40) Clays, K.; Persoons, A. Hyper-Rayleigh Scattering in Solution. *Phys. Rev. Lett.* **1991**, *66*, 2980.
- (41) Campo, J.; Desmet, F.; Wenseleers, W.; Goovaerts, E. Highly Sensitive Setup for Tunable Wavelength Hyper-Rayleigh Scattering with Parallel Detection and Calibration Data for Various Solvents. *Opt. Express* **2009**, *17*, 4587.
- (42) Oudar, J. L.; Chemla, D. S. Hyperpolarizabilities of the Nitroanilines and Their Relations to the Excited State Dipole Moment. *J. Chem. Phys.* **1977**, *66*, 2664.
- (43) te Velde, G.; Bickelhaupt, F. M.; Baerends, E. J.; Fonseca Guerra, C.; van Gisbergen, S. J. A.; Snijders, J. G.; Ziegler, T. Chemistry with ADF. *J. Comput. Chem.* **2001**, *22*, 931.
- (44) van Lenthe, E.; Baerends, E. J.; Snijders, J. G. Relativistic Regular Two-Component Hamiltonians. *J. Chem. Phys.* **1993**, *99*, 4597.
- (45) Van Leeuwen, R.; Baerends, E. J. Exchange-Correlation Potential with Correct Asymptotic Behavior. *Phys. Rev. A: At., Mol., Opt. Phys.* **1994**, *49*, 2421.
- (46) Cyvin, S. J.; Rauch, J. E.; Decius, J. C. Theory of Hyper-Raman Effects (Nonlinear Inelastic Light Scattering): Selection Rules and Depolarization Ratios for the Second-Order Polarizability. *J. Chem. Phys.* **1965**, *43*, 4083.
- (47) Willetts, A.; Rice, J. E.; Burland, D. M.; Shelton, D. P.; Willetts, A.; Rice, J. E. Problems in the Comparison of Theoretical and Experimental Hyperpolarizabilities. *J. Chem. Phys.* **1992**, *97*, 7590.
- (48) Pye, C. C.; Ziegler, T.; van Lenthe, E.; Louwen, J. N. An Implementation of the Conductor-like Screening Model of Solvation within the Amsterdam Density Functional Package—Part II. COSMO for Real Solvents 1. *Can. J. Chem.* **2009**, *87*, 790.

(49) Vila, F. D.; Strubbe, D. A.; Takimoto, Y.; Andrade, X.; Rubio, A.; Louie, S. G.; Rehr, J. J. Basis Set Effects on the Hyperpolarizability of  $\text{CHCl}_3$ : Gaussian-Type Orbitals, Numerical Basis Sets and Real-Space Grids. *J. Chem. Phys.* **2010**, *133*, 034111.

(50) Nappa, J.; Revillod, G.; Martin, G.; Russier-Antoine, I.; Benichou, E.; Jonin, C.; Brevet, P.-F. Second Harmonic Generation From Gold and Silver Nanoparticles In Liquid Suspensions. In *Non-Linear Optical Properties of Matter*; Papadopoulos, M. G., Sadlej, A. J., Leszczynski, J., Eds.; Springer: Berlin, Heidelberg, Germany, 2006; pp 645–669.

(51) Meng, X.; Xu, Q.; Wang, S.; Zhu, M. Ligand-Exchange Synthesis of Selenophenolate-Capped  $\text{Au}_{25}$  Nanoclusters. *Nanoscale* **2012**, *4*, 4161.

(52) Song, Y.; Zhong, J.; Yang, S.; Wang, S.; Cao, T.; Zhang, J.; Li, P.; Hu, D.; Pei, Y.; Zhu, M. Crystal Structure of  $\text{Au}_{25}(\text{SePh})_{18}$  Nanoclusters and Insights into Their Electronic, Optical and Catalytic Properties. *Nanoscale* **2014**, *6*, 13977.

(53) Song, Y.; Wang, S.; Zhang, J.; Kang, X.; Chen, S.; Li, P.; Sheng, H.; Zhu, M. Crystal Structure of Selenolate-Protected  $\text{Au}_{24}(\text{SeR})_{20}$  Nanocluster. *J. Am. Chem. Soc.* **2014**, *136*, 2963.

(54) Maity, P.; Takano, S.; Yamazoe, S.; Wakabayashi, T.; Tsukuda, T. Binding Motif of Terminal Alkynes on Gold Clusters. *J. Am. Chem. Soc.* **2013**, *135*, 9450.

(55) Wan, X.-K.; Yuan, S.-F.; Tang, Q.; Jiang, D.; Wang, Q.-M. Alkynyl-Protected  $\text{Au}_{23}$  Nanocluster: A 12-Electron System. *Angew. Chem., Int. Ed.* **2015**, *54*, 5977.

(56) Wang, Y.; Wan, X. K.; Ren, L.; Su, H.; Li, G.; Malola, S.; Lin, S.; Tang, Z.; Häkkinen, H.; Teo, B. K.; Wang, Q. M.; Zheng, N. Atomically Precise Alkynyl-Protected Metal Nanoclusters as a Model Catalyst: Observation of Promoting Effect of Surface Ligands on Catalysis by Metal Nanoparticles. *J. Am. Chem. Soc.* **2016**, *138*, 3278.

(57) Wan, X.-K.; Xu, W. W.; Yuan, S.-F.; Gao, Y.; Zeng, X.-C.; Wang, Q.-M. A Near-Infrared-Emissive Alkynyl-Protected  $\text{Au}_{24}$  Nanocluster. *Angew. Chem., Int. Ed.* **2015**, *54*, 9683.

(58) Yang, H.; Wang, Y.; Lei, J.; Shi, L.; Wu, X.; Makinen, V.; Lin, S.; Tang, Z.; He, J.; Häkkinen, H.; Zheng, L.; Zheng, N. Ligand-Stabilized  $\text{Au}_{13}\text{Cu}_x$  ( $x = 2, 4, 8$ ) Bimetallic Nanoclusters: Ligand Engineering to Control the Exposure of Metal Sites. *J. Am. Chem. Soc.* **2013**, *135*, 9568.

(59) Yang, H.; Wang, Y.; Zheng, N. Stabilizing Subnanometer  $\text{Ag}(0)$  Nanoclusters by Thiolate and Diphosphine Ligands and Their Crystal Structures. *Nanoscale* **2013**, *5*, 2674.